

# UCLA

## UCLA Previously Published Works

### Title

ORAI1 Limits SARS-CoV-2 Infection by Regulating Tonic Type I IFN Signaling

### Permalink

<https://escholarship.org/uc/item/9k6617h6>

### Journal

The Journal of Immunology, 208(1)

### ISSN

0022-1767

### Authors

Wu, Beibei  
Ramaiah, Arunachalam  
Garcia, Gustavo  
[et al.](#)

### Publication Date

2022

### DOI

10.4049/jimmunol.2100742

Peer reviewed



Published in final edited form as:

*J Immunol.* 2022 January 01; 208(1): 74–84. doi:10.4049/jimmunol.2100742.

## ORAI1 limits SARS-CoV-2 infection by regulating tonic type I interferon signaling

Beibei Wu<sup>1,#</sup>, Arunachalam Ramaiah<sup>2,3,#</sup>, Gustavo Garcia Jr.<sup>4</sup>, Spyridon Hasiakos<sup>1,5</sup>,  
Vaithilingaraja Arumugaswami<sup>4,6,7,8,\*</sup>, Sonal Srikanth<sup>1,8,\*</sup>

<sup>1</sup>Department of Physiology, David Geffen School of Medicine, University of California, Los Angeles, CA 90095, USA

<sup>2</sup>Department of Ecology and Evolutionary Biology, University of California, Irvine, CA 92697, USA

<sup>3</sup>Tata Institute for Genetics and Society, Center at inStem, Bangalore, KA, 560065, India

<sup>4</sup>Department of Molecular and Medical Pharmacology, David Geffen School of Medicine, University of California, Los Angeles, CA 90095, USA

<sup>5</sup>Division of Oral Biology and Medicine, UCLA School of Dentistry, Los Angeles, CA, USA.

<sup>6</sup>Eli and Edythe Broad Center of Regenerative Medicine and Stem Cell Research, University of California, Los Angeles, CA 90095, USA

<sup>7</sup>California NanoSystems Institute, University of California, Los Angeles, CA 90095, USA

<sup>8</sup>Senior authors

### Abstract

ORAI1 and STIM1 are the critical mediators of store-operated Ca<sup>2+</sup> entry by acting as the pore subunit and an endoplasmic reticulum-resident signaling molecule, respectively. In addition to Ca<sup>2+</sup> signaling, STIM1 is also involved in regulation of the type I interferon (IFN-I) response. To examine their potential role in SARS-CoV-2 infection, we generated *ORAI1* and *STIM1* knockout human HEK293-ACE2 cells and checked their responses. *STIM1* knockout cells showed strong resistance to SARS-CoV-2 infection due to enhanced type I interferon response. On the contrary, *ORAI1* deletion induced high susceptibility to SARS-CoV-2 infection. Mechanistically, *ORAI1* knockout cells showed reduced homeostatic cytoplasmic Ca<sup>2+</sup> concentration and severe impairment in tonic IFN-I signaling. Transcriptome analysis showed downregulation of multiple antiviral signaling pathways in *ORAI1* knockout cells, likely, due to reduced expression of the Ca<sup>2+</sup>-dependent transcription factors of the activator protein 1 (AP-1) family and *MEF2C*.

\* Address correspondence to: Dr. Sonal Srikanth, Department of Physiology, David Geffen School of Medicine, 53-266 CHS, 10833 Le Conte Avenue, Los Angeles, CA 90095, Tel: 310-794-2003; FAX: 310-206-5661, ssrikanth@mednet.ucla.edu, or, Dr. Vaithilingaraja Arumugaswami, B2-049A CHS, Box 956948, University of California, Los Angeles, CA 90095, Tel: 310 – 794-9568, varumugaswami@mednet.ucla.edu.

#Equal contribution

#### AUTHOR CONTRIBUTIONS

S.S. conceptualized the study, generated KO cells and performed imaging experiments. B.B.W. performed all the molecular biology and flow cytometry experiments and A.R. performed bioinformatics analysis of the RNA-seq data with help from S.H. G.G. and V.A. generated the SARS-CoV-2 virus and performed all infection experiments. S.S. wrote the manuscript with input from all authors.

#### COMPETING FINANCIAL INTERESTS

The authors do not have any competing financial interests.

Accordingly, modulation of homeostatic  $\text{Ca}^{2+}$  concentration by pre-treatment with ORAI1 blocker or agonist could influence baseline *IFNB* expression and resistance to SARS-CoV-2 infection in a human lung epithelial cell line. Our results identify a novel role of ORAI1-mediated  $\text{Ca}^{2+}$  signaling in regulating the tonic type I interferon levels, which determine host resistance to SARS-CoV-2 infection.

## Introduction

Type I Interferon (IFN-I) response provides the first line of defense against viral infection (1), and is also important for the development of adaptive immunity (2). IFN-I response is ubiquitous in almost all nucleated cells, whereas type III IFNs (IFN-III) are restricted to anatomic barriers and specific immune cells (3). This selectivity is due to the receptor expression patterns: IFN-I binds IFN- $\alpha$  receptor 1 (IFNAR1) and IFNAR2, which are ubiquitously expressed, while type III IFN binds IFN- $\lambda$  receptor 1 (IFNLR1) and IL10RB, which are preferentially expressed in epithelial cells (3). Despite using different receptors, IFN-I and IFN-III activate the same downstream signaling pathways and induce transcription of hundreds of IFN-stimulated genes (ISGs), with IFN-III inducing lower levels of ISG expression than IFN-I (4). The importance of IFN signaling pathway is underscored by the fact that most viruses have developed mechanisms to inactivate this pathway (5).

Coronavirus disease 2019 (COVID-19) pandemic is one of the worst crises of our times, prompting an urgent need to uncover host defense mechanisms to its causative agent, severe acute respiratory syndrome coronavirus 2 (SARS-CoV-2). SARS-CoV-2 utilizes multiple approaches to evade host IFN response, including suppression of IFN-I production as well as IFN-I signaling (6). The clinical manifestations and pathology of COVID-19 are similar to those of SARS-CoV-1, but the severities of the diseases differ (7). Unlike severe SARS-CoV-1 infection, SARS-CoV-2 infection shows a wide range of clinical features, ranging from asymptomatic, mild and moderate to severe and critical. The clinical manifestations of virus infection depend on virus-host interactions. Asymptomatic outcomes of SARS-CoV-2 infection may thus be attributed to strong host innate antiviral defense. In clinics, COVID-19 patients with circulating antibodies to IFN-I or loss-of-function mutations in genes necessary to mount the IFN-I response developed life-threatening pneumonia (8, 9). Recent studies have found that unlike original coronaviruses, SARS-CoV-2 is highly sensitive to pre-treatment with type I and III IFNs. Pre-treatment of immortalized or primary human airway epithelial cells with IFN-I or IFN-III imparts resistance to SARS-CoV-2 infection (10–12). Further, recent studies aiming at boosting IFN-I signaling, via pharmacological activation of stimulator of interferon genes (STING) robustly inhibited infection of multiple coronaviruses including SARS-CoV-2 in vitro as well as in vivo (13–16). Taken together, a picture emerges that tonic IFN-I signaling mediated by the baseline levels of IFN-I, that is known to prime the host antiviral status (17) can also provide a significant barrier to SARS-CoV-2 infection.

Store-operated  $\text{Ca}^{2+}$  entry (SOCE), induced by depletion of the endoplasmic reticulum (ER)  $\text{Ca}^{2+}$  stores after activation of G protein-coupled receptors or receptor tyrosine kinases,

is a ubiquitous mechanism of elevation of intracellular  $\text{Ca}^{2+}$  concentration ( $[\text{Ca}^{2+}]$ ) in most cell types.  $\text{Ca}^{2+}$  release-activated  $\text{Ca}^{2+}$  (CRAC) channels are a specialized class of store-operated  $\text{Ca}^{2+}$  (SOC) channels that play a primary role in the elevation of  $[\text{Ca}^{2+}]$  in immune cells (18, 19). CRAC channels consist of two major components, the plasma membrane (PM)-localized pore subunit, ORAI1, and an ER-resident  $\text{Ca}^{2+}$  sensor, stromal interaction molecule 1 (STIM1). STIM1 senses depletion of the ER  $\text{Ca}^{2+}$  stores and interacts with ORAI1 to open the pore.  $\text{Ca}^{2+}$  signaling mediated by CRAC channels is essential for induction of transcriptional programs via the NFAT (nuclear factor of activated T cells) pathway (18, 19). Severe combined immune deficiency (SCID) caused by mutations in *ORAI1* or *STIM1*, and the widespread clinical use of inhibitors of this pathway - cyclosporine A (CsA) and FK506 as immunosuppressants, underscore the importance of therapeutic targeting of the  $\text{Ca}^{2+}$ -NFAT pathway (18, 19).

While the current understanding of the role of ORAI1 is limited to  $\text{Ca}^{2+}$  signaling, a  $\text{Ca}^{2+}$  signaling-independent role of STIM1 in regulating the IFN-I response has been shown (20). Biochemical studies identified STIM1 as an interacting partner of STING, an ER-resident adaptor protein that plays a central role in cellular response to cytosolic DNA (21). It was shown that STIM1 forms a complex with STING on the ER membrane to prevent its aberrant activation in an SOCE-independent manner. Myeloid cell-specific *Stim1* knockout (KO) mice and a patient lacking STIM1 expression were shown to have elevated serum IFN- $\beta$  and increased expression of various ISGs (20, 22). Accordingly, myeloid-specific *Stim1* KO mice showed enhanced resistance to DNA virus infection, which was not observed in *Orai1* KO cells and mice (20). Here, we examined the role of *ORAI1* and *STIM1* in host resistance to infection with an RNA virus, SARS-CoV-2. Loss of ORAI1 markedly reduced the host resistance to SARS-CoV-2 by abolishing the baseline IFN- $\beta$  levels and impairing tonic IFN-I signaling. On the contrary, *STIM1* KO cells showed remarkable resistance to SARS-CoV-2 infection supporting previous studies of enhanced baseline IFN-I signaling (20). Our data suggest that tonic IFN-I signaling regulated by ORAI1 and STIM1 determines the cellular antiviral state and host resistance to SARS-CoV-2 infection.

## Materials and Methods

### Chemicals and Antibodies.

Fura 2-AM (F1221) was purchased from ThermoFisher Scientific. Thapsigargin and cyclosporin A were purchased from EMD Millipore. SARS-CoV Spike (S) antibodies - polyclonal anti-SARS coronavirus (BEI Resources: NR-10361 antiserum, Guinea Pig) was used for immunoblotting and monoclonal anti-SARS-CoV S protein antibody (BEI Resources: NR-616, similar to 240C) was used for immunocytochemistry. Antibodies for detection of human STIM1 (5668S) was purchased from Cell Signaling Technologies, that for detection of interferon alpha and beta receptor 1 (IFNAR-1) was purchased from Leinco Technologies, Inc. (I-400), that for detection of ORAI1 (ACC-060) was purchased from Alomone labs and that for detection of  $\beta$ -actin (sc-47778), was obtained from Santa Cruz Biotechnology. BTP2 and ionomycin were purchased from Millipore Sigma.

### Plasmids, sgRNAs and cells.

Human ACE2 coding sequence was cloned into a lentiviral vector as described (23). sgRNAs targeting human *ORAI1* (gRNA target sequence *GATCGGCCAGAGTTACTCC*) and human *STIM1* (*TGAGGATAAGCTCATCAGCG*) genes were subcloned into pLentiguide puro (Addgene). sgRNAs targeting human interferon alpha and beta receptor subunit 1 (IFNAR1) subcloned into pLentiCRISPR v2 was purchased from GenScript (catalog # IFNAR1 crRNA 1; gRNA target sequence *GGCGTGTTCAGACTGTTT*). Vero E6, HEK293 and A549 cells were obtained from the American Type Culture Collection center (ATCC, Manassas, VA). Vero cells were cultured in EMEM growth media (ATCC) supplemented with 10% (v/v) fetal bovine serum (FBS, Hyclone) and Penicillin/Streptomycin (Mediatech) at 37°C and 5% CO<sub>2</sub>. HEK293 cells were cultured in DMEM (Mediatech) supplemented with 10% (v/v) FBS (Hyclone), 2 mM L-glutamine (Mediatech), 10 mM HEPES (Mediatech) and Penicillin/Streptomycin (Mediatech) at 37°C and 5% CO<sub>2</sub>. A549 cells were cultured in Ham's F12-K (Kaighn's) medium (ThermoFisher) supplemented with 10% (v/v) FBS (Hyclone), 10 mM HEPES (Mediatech) and Penicillin/Streptomycin (Mediatech) at 37°C and 5% CO<sub>2</sub>.

### Virus.

SARS-CoV-2 (USA-WA1/2020) was obtained from BEI Resources of National Institute of Allergy and Infectious Diseases (NIAID). All the studies involving live virus was conducted in UCLA BSL3 high-containment facility. SARS-CoV-2 was passaged once in Vero E6 cells and viral stocks were aliquoted and stored at -80°C. Virus titer was measured in Vero E6 cells by established plaque assays.

### Lentiviral transduction of HEK293 and A549 cells.

To generate HEK293-ACE2 or A549-ACE2 cells, HEK293T cells were transfected with plasmid encoding ACE2 and packaging vectors (pMD2.G and psPAX2, Addgene) using calcium phosphate transfection method. Culture supernatants were harvested at 48 and 72 hours post transfection, filtered using a 0.45 µ PVDF filter and used for infection of HEK293 or A549 cells together with polybrene (8 µg/ml) using the spin-infection method. Transduced cells were selected with puromycin (1 µg/ml) 48 hours post second infection. For generation of *ORAI1*<sup>-/-</sup> and *STIM1*<sup>-/-</sup> cells, HEK293T cells were transfected with plasmids encoding sgRNA and packaging vectors as described above. Lentiviruses encoding Cas9 were generated using the same technique. Culture supernatants harvested at 48 and 72 hours post transfection were used for infection (50% of Cas9-encoding virus + 50% of sgRNA-encoding virus) of HEK293-ACE2 or A549-ACE2 cells together with polybrene (8 µg/ml) using the spin-infection method. Cells were selected with puromycin (1 µg/ml) and blasticidin (5 µg/ml) 48 hours post second infection.

### Endogenous ORAI1 staining and analysis.

For total endogenous ORAI1 detection, control, STIM1 KO and ORAI1 KO HEK293 (0.5 × 10<sup>6</sup>) were fixed with 4% PFA at room temperature for 15 mins, followed by permeabilization with PBS + 0.5% Igepal CA-630 and incubated with 1 µg unlabeled anti-ORAI1 antibody (ACC-060, Alomone labs) in PBS + 2% FBS + 0.5% Igepal CA-630.

Negative control sample did not contain the primary Ab. Cells were subsequently treated with FITC-conjugated secondary antibody, washed and data was acquired on a BD Fortessa flow cytometer (BD Biosciences) and analyzed using FlowJo software (Treestar Inc).

### Single-cell Ca<sup>2+</sup> imaging and immunofluorescence analysis.

HEK293-ACE cells were grown overnight on coverslips and loaded with 1  $\mu$ M Fura 2-AM for 40 min at 25°C for imaging. Intracellular [Ca<sup>2+</sup>]<sub>i</sub> measurements were performed using essentially the same methods as previously described (24). Briefly, microscopy was performed using an Olympus IX2 illumination system mounted on an Olympus IX51 inverted microscope using previously described methods (25). Acquisition and image analysis were performed using Slidebook (Intelligent Imaging Innovations, Inc.) software and graphs were plotted using Origin2020 (OriginLab). For immunofluorescence analysis, uninfected or SARS-CoV-2-infected cells were fixed for 20 mins with ice-cold methanol, permeabilized in buffer containing PBS + 0.2% Triton X-100, blocked with same buffer containing 2.5% goat serum, 2.5% donkey serum and 2% BSA. Cells were stained overnight in the blocking buffer with primary antibodies washed and treated with secondary antibody for 1 hour, stained for DAPI in permeabilization solution and visualized using 40X oil immersion lens and imaged using Slidebook 6.0 software (Intelligent Imaging Innovations, Inc.). Images were processed for enhancement of brightness or contrast using Slidebook 6.0 software.

### SARS-CoV-2 Infection.

Control, *ORAI1*<sup>-/-</sup>, or *STIM1*<sup>-/-</sup> HEK293-ACE2 cells or A549-ACE2 cells were seeded at  $1 \times 10^5$  cells per well in 0.4 ml volume in a 48-well plate, or  $5 \times 10^4$  cells per well in 0.2 ml volume in a 96-well plate. The following day, viral inoculum (MOI of 0.1 or 1.0 as indicated) was prepared using serum free media. The spent media from each well was removed and 100  $\mu$ l of prepared inoculum was added onto cells. For mock infection, serum free media (100  $\mu$ l/well) alone was added. The inoculated plates were incubated for 1 hour at 37°C with 5% CO<sub>2</sub>. The inoculum was spread by gently tilting the plate sideways every 15 minutes. At the end of incubation, the inoculum was replaced with serum supplemented media. At 20 hours post infection (hpi) the cells were either fixed with methanol for immunocytochemistry (ICC) analysis or harvested in TriZol reagent (ThermoFisher) for RNA-seq and RT-PCR analysis or lysed in RIPA lysis buffer for immunoblotting as described below.

### Plaque Assay.

Viral titers were determined by plaque assay on Vero E6 cells. Vero E6 cells were seeded in 12-well plates for 24 hours. Virus-containing supernatants were 10-fold serially diluted in PBS. The growth medium was removed from the cells, cells were washed once with PBS, and diluted supernatants were added (150  $\mu$ l/well). After 30 min inoculation, an overlay medium (double-concentrated minimal essential medium (MEM; supplemented with 2 % L-glutamine, 2 % Pen/Strep, 0.4 % bovine serum albumin (BSA)), mixed 1:1 with 2.5 % avicel solution (prepared in ddH<sub>2</sub>O)) was added to the cells (1.5 ml/well). Then, cells were incubated for 72 hours at 37 °C. After 72 hours, the overlay medium was removed from the cells, and following a washing step with 1x PBS the cells were fixed with 4 %

paraformaldehyde (PFA) for 30 min at 4 °C. Subsequently, the cells were counterstained with crystal violet solution to visualize the virus-induced plaques in the cell layer. The number of plaques at a given dilution were counted to calculate the viral titers as plaque-forming units (PFU/ml).

### RNA sample preparation and RT-qPCR.

Total RNA from cells harvested in TRIzol Reagent (ThermoFisher) was isolated using the Direct-zol RNA isolation kit (Zymo Research). RNA quantity and quality were confirmed with a NanoDrop ND-1000 spectrophotometer. cDNA was synthesized using 0.5–1.0 µg of total RNA using random hexamers and oligo(dT) primers and qScript cDNA Supermix (Quantabio). Real-time quantitative PCR was performed using iTaq Universal SYBR Green Supermix (Bio-Rad) and an iCycler IQ5 system (Bio-Rad) using gene-specific primers. Briefly, amplification was performed using 20 µl volume reactions in a 96-well plate format with the following conditions: 95°C for 30 sec for polymerase activation and cDNA denaturation, then 40 cycles at 95°C for 15 seconds and 60°C for 1 minute, with a melt-curve analysis at 65–95°C and 0.5°C increments at 2–5 seconds/step. Threshold cycles ( $C_T$ ) for all the candidate genes were normalized to those of 36B4 to obtain  $C_T$ . The specificity of primers was examined by melt-curve analysis and agarose gel electrophoresis of PCR products. Primer sequences are: *SARS-CoV-2*: (Forward: *GACCCCAAATCAGCGAAAT*, Reverse: *TCTGGTACTGCCAGTTGAATCTG*), human *ATF2* (Forward: *GCACAGCCACATCAGCTATT*, Reverse: *GGTGCCTGGGTGATTACAGT*); human *FOS* (Forward: *GGGCAAGGTGGAACAGTTAT*, Reverse: *CCGCTTGGAGTGTATCAGTCA*); human *MEF2C* (Forward: *GTATGGCAATCCCGAAACT*, Reverse: *ATCGTATTCTTGCTGCCTGG*), and human *36B4* (Forward: *AGATGCAGCAGATCCGCAT*, Reverse: *GTTCTTGCCCATCAGCACC*).

### Western Blot analysis.

Cells were lysed in RIPA lysis buffer (50 mM Tris pH 7.4, 1% NP-40, 0.25% sodium deoxycholate, 1 mM EDTA, 150 mM NaCl, 1 mM Na<sub>3</sub>VO<sub>4</sub>, 20 mM NaF, 1mM PMSF, 2 mg ml<sup>-1</sup> aprotinin, 2 mg ml<sup>-1</sup> leupeptin and 0.7 mg ml<sup>-1</sup> pepstatin) for 1 h with intermittent vortexing and centrifuged to remove debris. Samples were separated on 10% SDS-PAGE. Proteins were transferred to nitrocellulose membranes and subsequently analyzed by immunoblotting with relevant antibodies. Chemiluminescence images were acquired using an Image reader LAS-3000 LCD camera (FujiFilm).

### Cytokine measurement by ELISA.

For ELISA measurements under resting conditions, 1 million cells were cultured in low media volume to allow for concentration of cytokines. ELISA was performed on cell culture supernatants from indicated cells for detection of IFN-β (PBL Assay Science, #41410) or IL-6 (ThermoFisher Scientific, # 88-7066-22) using manufacturer's instructions.

### RNA sequencing and data analysis.

RNA was extracted with Direct-zol RNA Mini prep kit (Zymo Research). Libraries for RNA-Seq were prepared with TruSeq Stranded mRNA Library Prep Kit (Illumina). The

workflow consisted of mRNA enrichment and fragmentation. Cleaved RNA fragments were copied into first strand cDNA using reverse transcriptase and random primers. Strand specificity is achieved by replacing dTTP with dUTP, followed by second strand cDNA synthesis using DNA Polymerase I and RNase H. cDNA generation is followed by A-tailing, adaptor ligation and PCR amplification. Different adaptors were used for multiplexing samples in one lane. Sequencing was performed on Illumina HiSeq 3000 for SE 1×50 run. Data quality check was done on Illumina SAV. Demultiplexing was performed with Illumina Bcl2fastq v2.19.1.403 software. Raw reads for Orai1KO and STIM1KO SARS-CoV-2 infected samples (Orai1KO-SARS-CoV-2-3\_S18 and STIM1KO-SARS-CoV-2-1\_S19) were sampled down to 45 million reads before mapping. Illumina reads from all the samples were mapped to human and SARS-CoV-2 reference genomes by STAR v2.27a (26) and read counts per gene were quantified using human Ensembl GRCh38.98 and SARS-CoV-2 GTF file to generate raw reads counts. Differential expression analysis was performed using DESeq2 v1.28.1 in R v4.0.3 (27). Median of ratios method was used to normalize expression counts for each gene in all the experimental samples. Each gene in the samples was fitted into a negative binomial generalized linear model. Differentially expressed gene (DEG) candidates were considered if they were supported by a false discovery rate (FDR)  $P < 0.01$ . Unsupervised principal component analysis was performed using pcaExplorer (28) in R v4.0.3 (27). Reactome pathway analysis was performed for DEGs using human all genes as reference data set in the Reactome v65 (29) implemented in PANTHER. Reactome pathways were only considered if they were supported by FDR  $P < 0.05$ . The ggplot2 v3.3.2 in R and Prism GraphPad v8.4.3 were used to generate figures. The shinyheatmap web interface was used to prepare heat maps (30). The genes in the DEGs directly regulated by transcription factors (FOS, ATF2, MEF2C) were identified based on binding profiles of all public ChIP-seq data for particular gene loci from the CHIP-Atlas database (31). The regulated or target genes were accepted if the peak-call intervals of a given gene overlapped with a transcription start site (TSS)  $\pm 1$  Kb. RNA sequencing data are deposited in NCBI GEO under the accession number GSE173707 (<https://www.ncbi.nlm.nih.gov/geo/query/acc.cgi?acc=GSE173707>).

### Statistical analysis.

Statistical analysis was carried out using two-tailed Student's t-test. Differences were considered significant when  $p$  values were  $< 0.05$ . The hypergeometric test in R v4.0.3 was used to measure the statistical significance of the enriched genes in the DEGs regulated by transcription factors (FOS, ATF2, MEF2C) compared to regulated genes in the background gene sets of the human reference genome.

## Results

### Loss of ORAI1 reduces store-operated $\text{Ca}^{2+}$ entry and the baseline cytoplasmic $\text{Ca}^{2+}$ concentration in HEK293-ACE2 cells

To examine the role of ORAI1 and STIM1 in host response to SARS-CoV-2, we generated HEK293 cells stably expressing the receptor for SARS-CoV-2, angiotensin converting enzyme 2 (ACE2) (32). The resulting HEK293-ACE2 cells were transduced with lentiviruses encoding Cas9 and sgRNAs targeting either *ORAI1* or *STIM1*. All



three lines expressed similar levels of ACE2 as judged by immunocytochemistry and immunoblotting (Suppl. Figs. 1A and 1B). Loss of STIM1 protein expression was validated by immunoblotting, while that of ORAI1 was validated by flow cytometry (Figs. 1A and 1B). Multiple studies have shown loss of SOCE in HEK293 cells deleted for expression of *ORAI1/STIM1* (33, 34). To measure SOCE in *ORAI1*<sup>-/-</sup> and *STIM1*<sup>-/-</sup> HEK293-ACE2 cells, we used thapsigargin, a blocker of SERCA (sarco/endoplasmic reticulum Ca<sup>2+</sup>-ATPase) pump, that allows for passive depletion of the ER Ca<sup>2+</sup> stores, thereby activating SOCE. We observed almost complete abrogation of SOCE in both *ORAI1*<sup>-/-</sup> and *STIM1*<sup>-/-</sup> HEK293-ACE2 cells (Fig. 1C). While control cells showed a uniform increase in SOCE after re-introducing Ca<sup>2+</sup>-containing Ringer's solution, more than 95% of the polyclonal *ORAI1*<sup>-/-</sup> and *STIM1*<sup>-/-</sup> HEK293-ACE2 cells remained unresponsive. The Ca<sup>2+</sup> release from the ER in those cells was similar. Next, we checked whether loss of ORAI1/STIM1 affected resting cytoplasmic Ca<sup>2+</sup> concentration ([Ca<sup>2+</sup>]<sub>i</sub>) in unstimulated cells. Using our previously established protocols, we sequentially perfused the cells with 0 (Ca<sup>2+</sup>-free), 2, and 20 mM Ca<sup>2+</sup>-containing Ringer's solutions without any store depletion, to measure the homeostatic Ca<sup>2+</sup> levels in cells (25). Interestingly, in these measurements, only *ORAI1*<sup>-/-</sup> HEK293-ACE2 cells showed significant reduction in baseline [Ca<sup>2+</sup>]<sub>i</sub> in the presence of 2 or 20 mM Ca<sup>2+</sup>-containing Ringer's solution, suggesting an additional role of ORAI1 in regulating homeostatic [Ca<sup>2+</sup>]<sub>i</sub> in these cells (Fig. 1D). These data are in concurrence with previous observations where STIM2, a homolog of STIM1, was shown to be involved in maintaining resting intracellular [Ca<sup>2+</sup>]<sub>i</sub> ([Ca<sup>2+</sup>]<sub>i</sub>) together with ORAI1 (35). In those experiments, STIM2-depleted cells showed lowered resting [Ca<sup>2+</sup>]<sub>i</sub>, while those depleted for STIM1 had normal levels of resting [Ca<sup>2+</sup>]<sub>i</sub>. Collectively, by stable expression of ACE2 and deletion of *ORAI1/STIM1*, we developed a system to examine the role of ORAI1 and STIM1 in host responses to SARS-CoV-2 infection and uncovered the role of ORAI1 in Ca<sup>2+</sup> homeostasis in these cells.

### Loss of ORAI1 and STIM1 affects host resistance to SARS-CoV-2 infection

Next, we infected control, *ORAI1*<sup>-/-</sup>, and *STIM1*<sup>-/-</sup> HEK293-ACE2 cells with SARS-CoV-2 at two different multiplicity of infections (MOIs) – 0.1 and 1.0. Twenty hours after infection, cells were harvested to examine expression of viral proteins, as well as quantification of viral genome. We observed high levels of viral protein expression in SARS-CoV-2-infected *ORAI1*<sup>-/-</sup> HEK293-ACE2 cells when compared to control cells by immunoblotting (Fig. 2A), such that twenty hours after infection at high MOI (1.0), a significant fraction of the *ORAI1*<sup>-/-</sup> cells were lysed (Fig. 2B). On the contrary, *STIM1*<sup>-/-</sup> HEK293-ACE2 cells showed strong resistance to SARS-CoV-2 infection as judged by markedly reduced expression of viral protein both by immunoblotting and fewer plaques by immunocytochemistry when compared to control cells (Figs. 2A and 2B). Genome copy measurements at five hours after infection showed modestly increased and decreased susceptibility of *ORAI1*<sup>-/-</sup> and *STIM1*<sup>-/-</sup> cells, respectively, especially in cells infected at high MOI (Fig. 2C, left). Further, the increased and decreased susceptibility of *ORAI1*<sup>-/-</sup> and *STIM1*<sup>-/-</sup> cells, respectively, was obvious at twenty hours after infection, where *ORAI1*<sup>-/-</sup> cells showed ~100-fold increase in viral genome copy numbers whereas *STIM1*<sup>-/-</sup> cells showed more than 100-fold reduction, when compared to control HEK293-ACE2 cells (Fig. 2C, right). Taken together, these data show seemingly opposite phenotypes

of resistance and susceptibility to SARS-CoV-2 infection in *STIM1*<sup>-/-</sup> and *ORAI1*<sup>-/-</sup> cells, respectively.

### ***STIM1* KO cells exhibit resistance to SARS-CoV-2 infection due to higher baseline type I IFN response**

Based on our previous data showing pre-activation of the IFN-I pathway in *Stim1*<sup>-/-</sup> fibroblasts and macrophages (20), and high sensitivity of SARS-CoV-2 to IFN-I (10–12), we surmised that the resistance of *STIM1*<sup>-/-</sup> cells to SARS-CoV-2 infection was most likely derived from an increase in the baseline IFN-I response. As expected, *STIM1*<sup>-/-</sup> HEK293-ACE2 cells indeed showed higher levels of baseline IFN- $\beta$  levels, which remained elevated even after SARS-CoV-2 infection (Fig. 3A). We also observed enhanced IL-6 production by *STIM1*<sup>-/-</sup> cells under resting conditions and after SARS-CoV-2 infection when compared to control cells (Fig. 3B). Notably, these results showed that SARS-CoV-2 infection did not trigger a robust IFN-I response but induced strong IL-6 expression in consistency with previous observations (36).

To validate whether the resistance of *STIM1*<sup>-/-</sup> cells to SARS-CoV-2 infection was due to elevated IFN-I signaling, we generated HEK293-ACE2 cells deleted for both *STIM1* and *IFNAR1* using the CRISPR/Cas9 genome editing system (Fig. 3C). Deletion of *IFNAR1* abolished the increased baseline IFN- $\beta$  expression in *STIM1*<sup>-/-</sup> cells (Fig. 3D). In addition, co-deletion of *IFNAR1* abolished the resistance of *STIM1*<sup>-/-</sup> cells to SARS-CoV-2, as demonstrated by enhanced expression of viral proteins and increased burden of viral genome copies (Fig. 3E). These results suggest that the strong resistance of *STIM1*<sup>-/-</sup> cells to SARS-CoV-2 is predominantly derived from enhanced basal level of IFN- $\beta$ . Considering that SARS-CoV-2 did not trigger robust IFN-I signaling, these results also emphasize the importance of the basal IFN-I levels in host resistance to SARS-CoV-2 infection.

### **High susceptibility of *ORAI1* KO cells to SARS-CoV-2 infection is due to low baseline type I IFN signaling**

The increased susceptibility of *ORAI1*<sup>-/-</sup> cells to SARS-CoV-2 infection was surprising because ORAI1 deficiency did not influence host resistance to infection with a DNA virus, herpes simplex virus type 1 (HSV-1) in a previous study (20). Because SARS-CoV-2 is highly sensitive to the baseline IFN-I levels as observed in our analysis of *STIM1*<sup>-/-</sup> cells, we hypothesized that ORAI1 may influence the basal IFN-I levels. Culture supernatant analysis showed almost complete abrogation of baseline IFN- $\beta$  levels in *ORAI1*<sup>-/-</sup> cells when compared to control cells under resting conditions as well as upon infection with SARS-CoV-2 at low MOI (Fig. 4A). IL-6 levels in these cells were not influenced. In support of reduced IFN- $\beta$  levels, *ORAI1*<sup>-/-</sup> cells also showed reduced activation of the tonic IFN-I signaling pathway, including reduced basal levels of p-STAT1 as well as decrease in total STAT1 proteins (Fig. 4B), which has been proposed to be dependent on tonic IFN- $\beta$  signaling (17).

To check whether the high susceptibility of *ORAI1*<sup>-/-</sup> cells to SARS-CoV-2 infection was rescued by treatment with IFN- $\beta$ , we pre-treated these cells with low levels of IFN- $\beta$  for ~20 hours before SARS-CoV-2 infection. IFN- $\beta$  pre-treatment reduced the viral genome by

~10-fold in control cells, in agreement with other studies (10–12) (Fig. 4C). Importantly, pre-treatment of *ORAI1*<sup>-/-</sup> cells with IFN-β made the cells highly resistant, with more than 1,000-fold reduction in viral genome copy number, similar to the levels observed with control cells. These observations were validated by immunoblotting to check expression of viral proteins, where pre-treatment with IFN-β abrogated expression of viral proteins equally in control and *ORAI1*<sup>-/-</sup> cells (Fig. 4D). Since IFN-β pre-treatment in *ORAI1*<sup>-/-</sup> cells almost completely rescued the phenotypes to the level in control cells, these data suggest that reduced IFN-I baseline may have a significant contribution towards high susceptibility of *ORAI1*<sup>-/-</sup> cells to SARS-CoV-2 infection. Since the NFAT family of transcription factors are well-known downstream effectors of ORAI1-mediated SOCE, we checked whether reduced IFN-β levels in *ORAI1*<sup>-/-</sup> cells were due to loss of NFAT function. To check this possibility, we used CsA, which blocks calcineurin, a phosphatase necessary for de-phosphorylation of NFAT in the cytoplasm. We pretreated control and *ORAI1*<sup>-/-</sup> HEK293-ACE2 cells with CsA and examined its effect on the basal IFN-β production. Surprisingly, CsA treatment did not affect IFN-β levels in either of these cell types, suggesting a potential role of Ca<sup>2+</sup>-dependent transcription factors other than NFAT in this event (Fig. 4E).

### **ORAI1 acts on Ca<sup>2+</sup>-regulated transcription factors to modulate the baseline IFN-I production**

To uncover the antiviral defense mechanisms impaired in *ORAI1*<sup>-/-</sup> cells, we performed transcriptome analysis by bulk RNA sequencing of control, *ORAI1*<sup>-/-</sup>, and *STIM1*<sup>-/-</sup> HEK293-ACE2 cells before and 20 hours after SARS-CoV-2 infection (Suppl. Fig. 2). Among infected samples, viral count analysis showed uniform increase in expression of all the viral genes in *ORAI1*<sup>-/-</sup> cells, while the same was uniformly reduced in *STIM1*<sup>-/-</sup> cells, when compared to control cells (Fig. 5A). Importantly, the viral genome reads comprised ~20% of the total reads for control cells, ~77% for *ORAI1*<sup>-/-</sup> cells, and <1% for *STIM1*<sup>-/-</sup> cells, in concurrence with the observed phenotypes (Fig. 5B). Pathway enrichment analysis of *ORAI1*<sup>-/-</sup> cells before infection showed downregulation of multiple antiviral defense mechanisms, including ISG15 antiviral mechanism and MyD88 signaling pathways (Figs. 5C, D, and E). Transcriptome analysis further identified multiple transcription factors known to be involved in antiviral pathways, whose expression was altered by loss of *ORAI1* (Fig. 5F). Among the transcription factors that were significantly downregulated in *ORAI1*<sup>-/-</sup> cells, we identified *MEF2C* and members of the AP-1 family of transcription factors, *FOS*, *ATF2* and *JUN*. All of these transcription factors are known to be Ca<sup>2+</sup>-dependent for their functions (37–40). The AP-1 family of transcription factors, including FOS, JUN and ATF2, are known to bind the *IFNB* promoter to regulate its expression and JUN is also known to mediate tonic IFN signaling (17). Remarkably, promoter analysis showed profound enrichment of FOS, ATF2, MEF2C and JUN-binding sites among the differentially expressed genes in *ORAI1*<sup>-/-</sup> cells compared to the reference genome (Fig. 5G). Quantitative RT-PCR analysis confirmed downregulation of these transcription factors in *ORAI1*<sup>-/-</sup> cells under sterile conditions (Fig. 5H). Together, these data suggest that ORAI1 activity upregulates expression of the transcription factors *MEF2C*, *FOS*, *ATF2* and *JUN* leading to induction of multiple genes involved in antiviral defense mechanisms, including those involved in tonic IFN-I signaling, providing resistance to SARS-CoV-2 infection.

Recent studies using genome-wide CRISPR/cas9 knockout screens with SARS-CoV-2 infection have identified a plethora of host factors important for productive infection by SARS-CoV-2 (41–45). The list of necessary host factors required for SARS-CoV-2 propagation varied widely among the different screens, likely due to different cell types and infection conditions used for each screen. Not surprisingly, all the genome-wide screens identified ACE2, the receptor for SARS-CoV-2 as an essential factor for virus propagation. Our transcriptome analysis identified many of these host factors among the differentially expressed genes (DEGs) in *ORAI1*<sup>-/-</sup> cells (Suppl. Fig. 3). However, many of these factors were downregulated in *ORAI1*<sup>-/-</sup> cells, suggesting they may not play a significant role in high susceptibility to *ORAI1*<sup>-/-</sup> cells to SARS-CoV-2 infection. Collectively, these results suggest that ORAI1-mediated Ca<sup>2+</sup> signaling is mainly important for the regulation of tonic IFN-I levels, rather than host factors for SARS-CoV-2 infection.

### Pharmacological alteration of baseline [Ca<sup>2+</sup>]<sub>i</sub> modulates host resistance to SARS-CoV-2

Since SARS-CoV-2 infects the respiratory tract, we sought to validate our observations with human lung cells. We generated A549 cells stably expressing ACE-2 and deleted for expression of ORAI1 using the CRISPR/Cas9 genome editing system (Fig. 6A). Transcript analysis confirmed reduced expression of *IFNB* in *ORAI1*<sup>-/-</sup> A549-ACE2 cells (Fig. 6B). Next, we infected control and *ORAI1*<sup>-/-</sup> A549-ACE2 cells with SARS-CoV-2 and examined expression of viral proteins, as well as quantified expression of viral genome. Similar to our observations with HEK293-ACE2 cells, loss of ORAI1 imparted susceptibility to SARS-CoV-2 infection even in A549 cells, albeit to a lesser extent (Figs. 6C and 6D).

Recent studies focusing on identifying therapies for COVID-19 have found beneficial effects of IFN administration, especially at early stages of the disease, to reduce the severity and mortality associated with SARS-CoV-2 infections (46, 47). To check if pharmacological alteration of homeostatic [Ca<sup>2+</sup>]<sub>i</sub> affects host resistance to SARS-CoV-2, we pre-treated A549-ACE2 cells with various doses of a well-known blocker of ORAI1, BTP2 (chemical name: *N*-[4-[3,5-*Bis*(trifluoromethyl)-1*H*-pyrazol-1-yl]phenyl]-4-methyl-1,2,3-thiadiazole-5-carboxamide), for ~24 h to reduce homeostatic [Ca<sup>2+</sup>]<sub>i</sub>. Transcript analysis confirmed reduced expression of *IFNB* in blocker treated cells (Fig. 6E). Further, infection with SARS-CoV-2 showed increased viral protein expression and replication in cells treated with ORAI1 blocker, in concurrence with our observations with *ORAI1*<sup>-/-</sup> cells (Figs. 6F and 6G). Importantly, enhancing baseline [Ca<sup>2+</sup>]<sub>i</sub> by pre-treatment with low doses of an ionophore, ionomycin, elevated *IFNB* expression and imparted resistance to subsequent SARS-CoV-2 infection (Figs. 6H, 6I and 6J). These data show that enhancing baseline [Ca<sup>2+</sup>]<sub>i</sub> is sufficient to impart resistance to SARS-CoV-2 infection, most likely via boosting tonic IFN-I signaling.

## Discussion

The role of Ca<sup>2+</sup> signaling mediated by ORAI1 and STIM1 in adaptive immune cells (e.g., T and B cells) is well established (18, 19). Further, an earlier report suggested that loss of SOCE imparted susceptibility to IFN-I-induced cell death in Jurkat T cells (48). However, the function of this pathway in the host-pathogen responses in innate

immunity is poorly understood. A recent study had identified an important function of STIM1 in regulating the cytosolic DNA sensing pathway via direct interaction with STING independently from its role in  $\text{Ca}^{2+}$  signaling (20). The current study demonstrates a key role of ORAI1 in regulating tonic IFN- $\beta$  levels, thereby host response to SARS-CoV-2 infection by modulation of homeostatic cytoplasmic  $[\text{Ca}^{2+}]_i$ . Collectively, these studies uncover novel functions of CRAC channel components in the innate immune system.

Loss of STIM1 provides strong resistance to infection with HSV-1 by enhancing IFN-I signaling (20). The observation of resistance to virus infections in *STIM1*<sup>-/-</sup> cells has been extended to the current study using SARS-CoV-2. Abrogation of IFN-I signaling by co-deletion of IFNAR1 reduced baseline IFN- $\beta$  secretion and rendered *STIM1*<sup>-/-</sup> cells susceptible to SARS-CoV-2 infection, emphasizing the role of IFN-I in this resistance. Interestingly, loss of ORAI1 did not affect host resistance to HSV-1, most likely because the STING signaling pathway, which is predominantly important for sensing DNA viruses, was not impaired in *ORAI1*<sup>-/-</sup> cells (20). However, loss of ORAI1 resulted in very high susceptibility specifically to SARS-CoV-2 infection. In concurrence, pharmacological inhibition of ORAI1 to reduce homeostatic  $[\text{Ca}^{2+}]_i$  or enhancing homeostatic  $[\text{Ca}^{2+}]_i$  by pre-treatment with ionomycin modulated host susceptibility to SARS-CoV-2 infection. SARS-CoV-2 shows exceptionally high sensitivity to pre-treatment with type I or III IFNs, which profoundly reduces virus replication (10–12). Hence, reduction in tonic IFN- $\beta$  levels may enhance the susceptibility of *ORAI1*<sup>-/-</sup> cells especially to SARS-CoV-2 infection. It has been shown that in the absence of priming amounts of IFN- $\beta$ , mouse embryonic fibroblasts do not produce other IFN-I, suggesting that IFN- $\beta$  is a master regulator for all IFN-I activities and presumably those mediated by type III IFNs (49, 50). It has also been suggested that tonic IFN- $\beta$  signaling is required to maintain adequate expression of STAT1 and STAT2, and accordingly, the absence of tonic IFN- $\beta$  signaling reduces basal STAT expression (17), similar to our observation with *ORAI1*<sup>-/-</sup> cells (Fig. 4B). Besides, loss of ORAI1 was shown to downregulate multiple pathways including, ISG antiviral signaling, TLR7/8 signaling as well as MyD88 signaling cascades involved in RNA sensing. Collectively, loss of tonic IFN-I signaling in combination with impaired function of other antiviral signaling cascades is likely to contribute towards the exquisite sensitivity of *ORAI1*<sup>-/-</sup> cells to SARS-CoV-2.

The *IFNB* promoter contains four positive regulatory domains (PRDI-PRDIV), which are occupied by overlapping transcription factor complexes. Interferon regulatory factor 3 (IRF3) and IRF7 bind PRDI and III; the NF- $\kappa$ B RelA-p50 heterodimer binds PRDII; and the AP-1 heterodimer of ATF-2 and c-Jun binds PRDIV. The binding of each of these components in the correct orientation and location results in activation of the *IFNB* promoter in response to virus infection (17). Tonic IFN- $\beta$  expression is independent of IRF3 and IRF7 but instead depends on the c-Jun and NF- $\kappa$ B p50 subunit. *ORAI1*<sup>-/-</sup> cells showed reduced expression of multiple AP-1 family transcription factors, including ATF-2, FOS and JUN, as well as the NF- $\kappa$ B p50 subunit, which are likely to contribute to reduced baseline IFN- $\beta$  levels in these cells. Notably, while SOCE was abolished in both *ORAI1*<sup>-/-</sup> and *STIM1*<sup>-/-</sup> cells, the baseline  $[\text{Ca}^{2+}]_i$  was reduced only in *ORAI1*<sup>-/-</sup> cells. Based on the previous finding that STIM2, that has a lower binding affinity to  $\text{Ca}^{2+}$  than STIM1, is crucial for regulation of homeostatic  $\text{Ca}^{2+}$  levels (35), it is expected that *STIM2*<sup>-/-</sup> cells may have

lower tonic IFN-I signaling, thereby high susceptibility to SARS-CoV-2 infection similar to *ORAI1*<sup>-/-</sup> cells. Another notable difference between ORAI1 and STIM1 deficiency is differential expression of IFN- $\beta$  and IL-6. *STIM1*<sup>-/-</sup> cells showed enhanced expression of both these cytokines, in consistence with the observation that activation of the STING pathway upregulates expression of both IFN- $\beta$  and IL-6 (20, 21). However, *ORAI1*<sup>-/-</sup> cells had normal expression of IL-6, but still showed high susceptibility to SARS-CoV-2 infection, suggesting that the protective effect of STIM1 deficiency is predominantly derived from increased levels of IFN- $\beta$ . Therefore, these results obtained from the analysis of *ORAI1*<sup>-/-</sup> and *STIM1*<sup>-/-</sup> cells cohesively suggest that tonic IFN-I signaling is a crucial determinant for the degree of host resistance to SARS-CoV-2.

In summary, we examined the role of CRAC channel components, ORAI1 and STIM1, in host resistance to SARS-CoV-2 infection. *STIM1*<sup>-/-</sup> cells showed remarkable resistance to SARS-CoV-2 infection supporting previous studies of the role of elevated baseline IFN-I levels (20). Loss of ORAI1 severely impaired the tonic IFN-I levels, thereby reducing resistance to SARS-CoV-2 infection. Mechanistically, ORAI1-mediated Ca<sup>2+</sup> signaling affects expression of various transcription factors, including *FOS*, *JUN*, *ATF2*, and *MEF2C*, that regulate multiple host defense pathways. The key finding of this study is that the baseline IFN- $\beta$  level regulated by ORAI1-mediated Ca<sup>2+</sup> signaling is critical for priming the cellular antiviral state, thereby determining host resistance to SARS-CoV-2 infection. A recent phase 2 clinical trial of inhaled, nebulized IFN- $\beta$  to treat people with COVID-19 resulted in accelerated recovery, supporting localized delivery of IFN-I as a potential prophylactic and therapeutic agent against COVID-19 (47). The therapeutic effect of IFN-I targeting SARS-CoV-2 infection may be partly derived from boosting tonic IFN-I signaling. Our findings may help develop novel therapeutic methods to combat SARS-CoV-2 infection by demonstrating that pharmacological enhancement of baseline cytoplasmic [Ca<sup>2+</sup>] improved host resistance to SARS-CoV-2. Furthermore, the current study emphasizing the crucial role of tonic IFN-I signaling in resistance to SARS-CoV-2 infection may guide future identification of vulnerable populations and targeted therapies at boosting tonic IFN-I signaling.

## Supplementary Material

Refer to Web version on PubMed Central for supplementary material.

## ACKNOWLEDGEMENTS

The authors thank Barbara Dillon, UCLA High-Containment Program Director for BSL3 work. The authors would also like to thank Yousang Gwack (UCLA) for helpful suggestions and Shawn Cokus (UCLA Collaboratory Fellow) for suggestions about statistical analysis of transcription factor enrichment data.

### Funding Sources:

This work was supported by the National Institute of Health grants AI146352 (S.S.), EY032149 (V.A.), Broad Stem cell Research Center institutional awards OCRC 20-76 (S.S.) and OCRC 20-15 (V.A.), and the California Institute for Regenerative Medicine Tran Award, TRANICOVID19-11975 (V.A.). A.R. is supported by the Tata Institute for Genetics and Society.

## References

1. tenOever BR 2016. The Evolution of Antiviral Defense Systems. *Cell Host Microbe* 19: 142–149. [PubMed: 26867173]
2. Iwasaki A, and Medzhitov R. 2015. Control of adaptive immunity by the innate immune system. *Nat Immunol* 16: 343–353. [PubMed: 25789684]
3. Lazear HM, Schoggins JW, and Diamond MS. 2019. Shared and Distinct Functions of Type I and Type III Interferons. *Immunity* 50: 907–923. [PubMed: 30995506]
4. Crotta S, Davidson S, Mahlakoiv T, Desmet CJ, Buckwalter MR, Albert ML, Staeheli P, and Wack A. 2013. Type I and type III interferons drive redundant amplification loops to induce a transcriptional signature in influenza-infected airway epithelia. *PLoS Pathog* 9: e1003773. [PubMed: 24278020]
5. Schulz KS, and Mossman KL. 2016. Viral Evasion Strategies in Type I IFN Signaling - A Summary of Recent Developments. *Front Immunol* 7: 498. [PubMed: 27891131]
6. Xia H, and Shi PY. 2020. Antagonism of Type I Interferon by Severe Acute Respiratory Syndrome Coronavirus 2. *J Interferon Cytokine Res* 40: 543–548. [PubMed: 33337934]
7. Xie M, and Chen Q. 2020. Insight into 2019 novel coronavirus - An updated interim review and lessons from SARS-CoV and MERS-CoV. *Int J Infect Dis* 94: 119–124. [PubMed: 32247050]
8. Bastard P, Rosen LB, Zhang Q, Michailidis E, Hoffmann HH, Zhang Y, Dorgham K, Philippot Q, Rosain J, Beziat V, Manry J, Shaw E, Haljasmagi L, Peterson P, Lorenzo L, Bizien L, Trouillet-Assant S, Dobbs K, de Jesus AA, Belot A, Kallaste A, Catherinot E, Tandjaoui-Lambiotte Y, Le Pen J, Kerner G, Bigio B, Seeleuthner Y, Yang R, Bolze A, Spaan AN, Delmonte OM, Abers MS, Aiuti A, Casari G, Lampasona V, Piemonti L, Ciceri F, Bilguvar K, Lifton RP, Vasse M, Smadja DM, Migaud M, Hadjadj J, Terrier B, Duffy D, Quintana-Murci L, van de Beek D, Roussel L, Vinh DC, Tangye SG, Haerynck F, Dalmau D, Martinez-Picado J, Brodin P, Nussenzweig MC, Boisson-Dupuis S, Rodriguez-Gallego C, Vogt G, Mogensen TH, Oler AJ, Gu J, Burbelo PD, Cohen JI, Biondi A, Bettini LR, D'Angio M, Bonfanti P, Rossignol P, Mayaux J, Rieux-Laucat F, Husebye ES, Fusco F, Ursini MV, Imberti L, Sottini A, Paghera S, Quiros-Roldan E, Rossi C, Castagnoli R, Montagna D, Licari A, Marseglia GL, Duval X, Ghosn J, H. Lab, N.-U. I. R. t. C. Group, C. Clinicians, C.-S. Clinicians, C. G. Imagine, C. C. S. G. French, C. Milieu Interieur, V. C. C. Co, U. M. C. C.-B. Amsterdam, C. H. G. Effort, Tsang JS, Goldbach-Mansky R, Kisand K, Lionakis MS, Puel A, Zhang SY, Holland SM, Gorochov G, Jouanguy E, Rice CM, Cobat A, Notarangelo LD, Abel, Su HC, and Casanova JL. 2020. Autoantibodies against type I IFNs in patients with life-threatening COVID-19. *Science* 370.
9. Zhang Q, Bastard P, Liu Z, Le Pen J, Moncada-Velez M, Chen J, Ogishi M, Sabli IKD, Hodeib S, Korol C, Rosain J, Bilguvar K, Ye J, Bolze A, Bigio B, Yang R, Arias AA, Zhou Q, Zhang Y, Onodi F, Korniotis S, Karpf L, Philippot Q, Chbihi M, Bonnet-Madin L, Dorgham K, Smith N, Schneider WM, Razoooky BS, Hoffmann HH, Michailidis E, Moens L, Han JE, Lorenzo L, Bizien L, Meade P, Neehus AL, Ugurbil AC, Corneau A, Kerner G, Zhang P, Rapaport F, Seeleuthner Y, Manry J, Masson C, Schmitt Y, Schluter A, Le Voyer T, Khan T, Li J, Fellay J, Roussel L, Shahrooei M, Alosaimi MF, Mansouri D, Al-Saud H, Al-Mulla F, Almourfi F, Al-Muhsen SZ, Alsohime F, Al Turki S, Hasanato R, van de Beek D, Biondi A, Bettini LR, D'Angio M, Bonfanti P, Imberti L, Sottini A, Paghera S, Quiros-Roldan E, Rossi C, Oler AJ, Tompkins MF, Alba C, Vandernoot I, Goffard JC, Smits G, Migeotte I, Haerynck F, Soler-Palacin P, Martin-Nalda A, Colobran R, Morange PE, Keles S, Colkesen F, Ozcelik T, Yasar KK, Senoglu S, Karabela SN, Rodriguez-Gallego C, Novelli G, Hraiech S, Tandjaoui-Lambiotte Y, Duval X, Laouenan C, Clinicians C-S, Clinicians C, Imagine CG, French CCSG, Co VCC, Amsterdam UMCC-B, Effort CHG, Group N-UTCI, Snow AL, Dalgard CL, Milner JD, Vinh DC, Mogensen TH, Marr N, Spaan AN, Boisson B, Boisson-Dupuis S, Bustamante J, Puel A, Ciancanelli MJ, Meyts I, Maniatis T, Soumelis V, Amara A, Nussenzweig M, Garcia-Sastre A, Krammer F, Pujol A, Duffy D, Lifton RP, Zhang SY, Gorochov G, Beziat V, Jouanguy E, Sancho-Shimizu V, Rice CM, Abel L, Notarangelo LD, Cobat A, Su HC, and Casanova JL. 2020. Inborn errors of type I IFN immunity in patients with life-threatening COVID-19. *Science* 370.
10. Vanderheiden A, Ralfs P, Chirkova T, Upadhyay AA, Zimmerman MG, Bedoya S, Aoued H, Tharp GM, Pellegrini KL, Manfredi C, Sorscher E, Mainou B, Lobby JL, Kohlmeier JE, Lowen AC, Shi

- PY, Menachery VD, Anderson LJ, Grakoui A, Bosinger SE, and Suthar MS. 2020. Type I and Type III Interferons Restrict SARS-CoV-2 Infection of Human Airway Epithelial Cultures. *J Virol* 94.
11. Lokugamage KG, Hage A, de Vries M, Valero-Jimenez AM, Schindewolf C, Dittmann M, Rajsbaum R, and Menachery VD. 2020. Type I Interferon Susceptibility Distinguishes SARS-CoV-2 from SARS-CoV. *J Virol* 94.
  12. Blanco-Melo D, Nilsson-Payant BE, Liu WC, Uhl S, Hoagland D, Moller R, Jordan TX, Oishi K, Panis M, Sachs D, Wang TT, Schwartz RE, Lim JK, Albrecht RA, and tenOever BR. 2020. Imbalanced Host Response to SARS-CoV-2 Drives Development of COVID-19. *Cell* 181: 1036–1045 e1039. [PubMed: 32416070]
  13. Humphries F S.-G. L; Jiang Z; Wilson R; Landis P; Ng SL; Parsi KM; Maehr R; Cruz J; Morales-Ramos A; Ramanjulu J; Bertin J; Pesiridis GS; Fitzgerald K 2021. A diamidobenzimidazole STING agonist protects against SARS-CoV-2 infection. *Sci Immunol* 6.
  14. Li M F. M; Ying B; Descamps H; Lee E; Dittmar M; Lee JS; Whig K; Kamalia B; Dohnalova L; Uhr G; Zarkoob H; Chen Y; Ramage H; Ferrer M; Lynch K; Schultz D; Thaiss C; Diamond M; and Cherry S 2021. Pharmacological activation of STING blocks SARS-CoV-2 infection. *Sci Immunol* 6.
  15. Liu W, Reyes HM, Yang JF, Li Y, Stewart KM, Basil MC, Lin SM, Katzen J, Morrisey EE, Weiss SR, and You J. 2021. Activation of STING Signaling Pathway Effectively Blocks Human Coronavirus Infection. *J Virol* 95.
  16. Zhu Q, Zhang Y, Wang L, Yao X, Wu D, Cheng J, Pan X, Liu H, Yan Z, and Gao L. 2021. Inhibition of coronavirus infection by a synthetic STING agonist in primary human airway system. *Antiviral Res* 187: 105015. [PubMed: 33444702]
  17. Gough DJ, Messina NL, Clarke CJ, Johnstone RW, and Levy DE. 2012. Constitutive type I interferon modulates homeostatic balance through tonic signaling. *Immunity* 36: 166–174. [PubMed: 22365663]
  18. Srikanth S, and Gwack Y. 2013. Orai1-NFAT signalling pathway triggered by T cell receptor stimulation. *Mol Cells* 35: 182–194. [PubMed: 23483280]
  19. Prakriya M, and Lewis RS. 2015. Store-Operated Calcium Channels. *Physiol Rev* 95: 1383–1436. [PubMed: 26400989]
  20. Srikanth S, Woo JS, Wu B, El-Sherbiny YM, Leung J, Chupradit K, Rice L, Seo GJ, Calmettes G, Ramakrishna C, Cantin E, An DS, Sun R, Wu TT, Jung JU, Savic S, and Gwack Y. 2019. The Ca(2+) sensor STIM1 regulates the type I interferon response by retaining the signaling adaptor STING at the endoplasmic reticulum. *Nat Immunol* 20: 152–162. [PubMed: 30643259]
  21. Hopfner KP, and Hornung V. 2020. Molecular mechanisms and cellular functions of cGAS-STING signalling. *Nat Rev Mol Cell Biol* 21: 501–521. [PubMed: 32424334]
  22. Rice L, Stockdale C, Berry I, O’Riordan S, Pysden K, Anwar R, Rushambuza R, Blyth M, Srikanth S, Gwack Y, El-Sherbiny YM, Carter C, and Savic S. 2019. A Report of Novel STIM1 Deficiency and 6-Year Follow-Up of Two Previous Cases Associated with Mild Immunological Phenotype. *J Clin Immunol*.
  23. Garcia G Jr., Sharma A, Ramaiah A, Sen C, Purkayastha A, Kohn DB, Parcels MS, Beck S, Kim H, Bakowski MA, Kirkpatrick MG, Riva L, Wolff KC, Han B, Yuen C, Ulmert D, Purbey PK, Scumpia P, Beutler N, Rogers TF, Chatterjee AK, Gabriel G, Bartenschlager R, Gomperts B, Svendsen CN, Betz UAK, Damoiseaux RD, and Arumugaswami V. 2021. Antiviral drug screen identifies DNA-damage response inhibitor as potent blocker of SARS-CoV-2 replication. *Cell Rep*: 108940. [PubMed: 33784499]
  24. Srikanth S, Jung HJ, Ribalet B, and Gwack Y. 2010. The intracellular loop of Orai1 plays a central role in fast inactivation of Ca<sup>2+</sup> release-activated Ca<sup>2+</sup> channels. *J Biol Chem* 285: 5066–5075. [PubMed: 20007711]
  25. Srikanth S, Jung HJ, Kim KD, Souda P, Whitelegge J, and Gwack Y. 2010. A novel EF-hand protein, CRACR2A, is a cytosolic Ca<sup>2+</sup> sensor that stabilizes CRAC channels in T cells. *Nat Cell Biol* 12: 436–446. [PubMed: 20418871]



26. Dobin A, Davis CA, Schlesinger F, Drenkow J, Zaleski C, Jha S, Batut P, Chaisson M, and Gingeras TR. 2013. STAR: ultrafast universal RNA-seq aligner. *Bioinformatics* 29: 15–21. [PubMed: 23104886]
27. Love MI, Huber W, and Anders S. 2014. Moderated estimation of fold change and dispersion for RNA-seq data with DESeq2. *Genome Biol* 15: 550. [PubMed: 25516281]
28. Marini F, and Binder H. 2019. pcaExplorer: an R/Bioconductor package for interacting with RNA-seq principal components. *BMC Bioinformatics* 20: 331. [PubMed: 31195976]
29. Jassal B, Matthews L, Viteri G, Gong C, Lorente P, Fabregat A, Sidiropoulos K, Cook J, Gillespie M, Haw R, Loney F, May B, Milacic M, Rothfels K, Sevilla C, Shamovsky V, Shorsler S, Varusai T, Weiser J, Wu G, Stein L, Hermjakob H, and D'Eustachio P. 2020. The reactome pathway knowledgebase. *Nucleic Acids Res* 48: D498–D503. [PubMed: 31691815]
30. Khomtchouk BB, Hennessy JR, and Wahlestedt C. 2017. shinyheatmap: Ultra fast low memory heatmap web interface for big data genomics. *PLoS One* 12: e0176334. [PubMed: 28493881]
31. Oki S, Ohta T, Shioi G, Hatanaka H, Ogasawara O, Okuda Y, Kawaji H, Nakaki R, Sese J, and Meno C. 2018. ChIP-Atlas: a data-mining suite powered by full integration of public ChIP-seq data. *EMBO Rep* 19.
32. Li W, Moore MJ, Vasileva N, Sui J, Wong SK, Berne MA, Somasundaran M, Sullivan JL, Luzuriaga K, Greenough TC, Choe H, and Farzan M. 2003. Angiotensin-converting enzyme 2 is a functional receptor for the SARS coronavirus. *Nature* 426: 450–454. [PubMed: 14647384]
33. Nomura A, Yokoe S, Tomoda K, Nakagawa T, Martin-Romero FJ, and Asahi M. 2020. Fluctuation in O-GlcNAcylation inactivates STIM1 to reduce store-operated calcium ion entry via down-regulation of Ser(621) phosphorylation. *J Biol Chem* 295: 17071–17082. [PubMed: 33023909]
34. Yeast RE, Emrich SM, Zhang X, Xin P, Johnson MT, Fike AJ, Walter V, Hempel N, Yule DI, Sneyd J, Gill DL, and Trebak M. 2020. The native ORAI channel trio underlies the diversity of Ca(2+) signaling events. *Nat Commun* 11: 2444. [PubMed: 32415068]
35. Brandman O, Liou J, Park WS, and Meyer T. 2007. STIM2 is a feedback regulator that stabilizes basal cytosolic and endoplasmic reticulum Ca2+ levels. *Cell* 131: 1327–1339. [PubMed: 18160041]
36. Chen G, Wu D, Guo W, Cao Y, Huang D, Wang H, Wang T, Zhang X, Chen H, Yu H, Zhang X, Zhang M, Wu S, Song J, Chen T, Han M, Li S, Luo X, Zhao J, and Ning Q. 2020. Clinical and immunological features of severe and moderate coronavirus disease 2019. *J Clin Invest* 130: 2620–2629. [PubMed: 32217835]
37. Ng SW, Nelson C, and Parekh AB. 2009. Coupling of Ca(2+) microdomains to spatially and temporally distinct cellular responses by the tyrosine kinase Syk. *J Biol Chem* 284: 24767–24772. [PubMed: 19584058]
38. McKinsey TA, Zhang CL, and Olson EN. 2002. MEF2: a calcium-dependent regulator of cell division, differentiation and death. *Trends Biochem Sci* 27: 40–47. [PubMed: 11796223]
39. Lesch A, Hui X, Lipp P, and Thiel G. 2015. Transient receptor potential melastatin-3 (TRPM3)-induced activation of AP-1 requires Ca2+ ions and the transcription factors c-Jun, ATF2, and ternary complex factor. *Mol Pharmacol* 87: 617–628. [PubMed: 25576487]
40. Ban N, Yamada Y, Someya Y, Ihara Y, Adachi T, Kubota A, Watanabe R, Kuroe A, Inada A, Miyawaki K, Sunaga Y, Shen ZP, Iwakura T, Tsukiyama K, Toyokuni S, Tsuda K, and Seino Y. 2000. Activating transcription factor-2 is a positive regulator in CaM kinase IV-induced human insulin gene expression. *Diabetes* 49: 1142–1148. [PubMed: 10909971]
41. Hoffmann HH, Schneider WM, Rozen-Gagnon K, Miles LA, Schuster F, Razoooky B, Jacobson E, Wu X, Yi S, Rudin CM, MacDonald MR, McMullan LK, Poirier JT, and Rice CM. 2021. TMEM41B Is a Pan-flavivirus Host Factor. *Cell* 184: 133–148 e120. [PubMed: 33338421]
42. Schneider WM, Luna JM, Hoffmann HH, Sanchez-Rivera FJ, Leal AA, Ashbrook AW, Le Pen J, Ricardo-Lax I, Michailidis E, Peace A, Stenzel AF, Lowe SW, MacDonald MR, Rice CM, and Poirier JT. 2021. Genome-Scale Identification of SARS-CoV-2 and Pan-coronavirus Host Factor Networks. *Cell* 184: 120–132 e114. [PubMed: 33382968]
43. Wang R, Simoneau CR, Kulsuptrakul J, Bouhaddou M, Travisano KA, Hayashi JM, Carlson-Stevermer J, Zengel JR, Richards CM, Fozouni P, Oki J, Rodriguez L, Joehnk B, Walcott K, Holden K, Sil A, Carette JE, Krogan NJ, Ott M, and Puschnik AS. 2021. Genetic Screens

- Identify Host Factors for SARS-CoV-2 and Common Cold Coronaviruses. *Cell* 184: 106–119 e114. [PubMed: 33333024]
44. Wei J, Alfajaro MM, DeWeirdt PC, Hanna RE, Lu-Culligan WJ, Cai WL, Strine MS, Zhang SM, Graziano VR, Schmitz CO, Chen JS, Mankowski MC, Filler RB, Ravindra NG, Gasque V, de Miguel FJ, Patil A, Chen H, Oguntuyo KY, Abriola L, Surovtseva YV, Orchard RC, Lee B, Lindenbach BD, Politi K, van Dijk D, Kadoch C, Simon MD, Yan Q, Doench JG, and Wilen CB. 2021. Genome-wide CRISPR Screens Reveal Host Factors Critical for SARS-CoV-2 Infection. *Cell* 184: 76–91 e13. [PubMed: 33147444]
  45. Daniloski Z, Jordan TX, Wessels HH, Hoagland DA, Kasela S, Legut M, Maniatis S, Mimitou EP, Lu L, Geller E, Danziger O, Rosenberg BR, Phatnani H, Smibert P, Lappalainen T, tenOever BR, and Sanjana NE. 2021. Identification of Required Host Factors for SARS-CoV-2 Infection in Human Cells. *Cell* 184: 92–105 e116. [PubMed: 33147445]
  46. Hoagland DA, Moller R, Uhl SA, Oishi K, Frere J, Golyner I, Horiuchi S, Panis M, Blanco-Melo D, Sachs D, Arkun K, Lim JK, and tenOever BR. 2021. Leveraging the antiviral type I interferon system as a first line of defense against SARS-CoV-2 pathogenicity. *Immunity* 54: 557–570 e555. [PubMed: 33577760]
  47. Monk PD, Marsden RJ, Tear VJ, Brookes J, Batten TN, Mankowski M, Gabbay FJ, Davies DE, Holgate ST, Ho LP, Clark T, Djukanovic R, Wilkinson TMA, and Inhaled Interferon Beta C-SG. 2021. Safety and efficacy of inhaled nebulised interferon beta-1a (SNG001) for treatment of SARS-CoV-2 infection: a randomised, double-blind, placebo-controlled, phase 2 trial. *Lancet Respir Med* 9: 196–206. [PubMed: 33189161]
  48. Yue C, Soboloff J, and Gamero AM. 2012. Control of type I interferon-induced cell death by Orai1-mediated calcium entry in T cells. *J Biol Chem* 287: 3207–3216. [PubMed: 22144678]
  49. Takaoka A, Mitani Y, Suemori H, Sato M, Yokochi T, Noguchi S, Tanaka N, and Taniguchi T. 2000. Cross talk between interferon-gamma and -alpha/beta signaling components in caveolar membrane domains. *Science* 288: 2357–2360. [PubMed: 10875919]
  50. Erlandsson L, Blumenthal R, Eloranta ML, Engel H, Alm G, Weiss S, and Leanderson T. 1998. Interferon-beta is required for interferon-alpha production in mouse fibroblasts. *Curr Biol* 8: 223–226. [PubMed: 9501984]

**Key Points**

ORAI1 regulates tonic IFN-I signaling via modulating baseline  $Ca^{2+}$  levels  
Deletion of ORAI1 enhances host susceptibility to SARS-CoV-2 infection

Author Manuscript

Author Manuscript

Author Manuscript

Author Manuscript

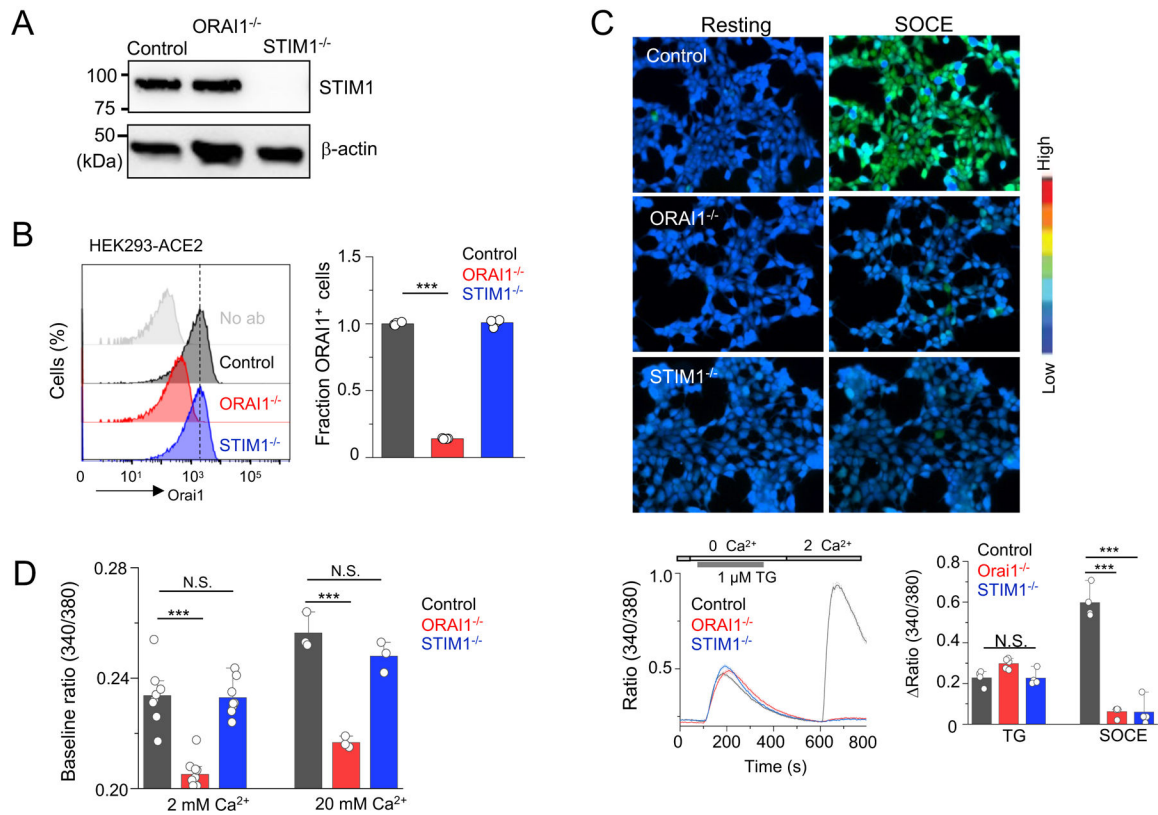


**Figure 1. Loss of ORAI1 reduces basal Ca<sup>2+</sup> concentration and abrogates SOCE in HEK293-ACE2 cells**

(A) Representative immunoblot showing expression of STIM1 in lysates from control, *ORAI1*<sup>-/-</sup>, or *STIM1*<sup>-/-</sup> HEK293-ACE2 cells.  $\beta$ -actin – loading control. Data are representative of two independent experiments.

(B) Representative histograms showing levels of total ORAI1 protein in control, *ORAI1*<sup>-/-</sup>, and *STIM1*<sup>-/-</sup> HEK293-ACE2 cells after permeabilization and intracellular staining with anti-ORAI1 antibody. The bar graph shows average ( $\pm$  s.e.m.) from three independent experiments.

(C) Representative pseudocoloured epifluorescence images of indicated cells under resting conditions or at the peak of SOCE. Below - Representative traces showing averaged SOCE from control (39 cells), *ORAI1*<sup>-/-</sup> (35 cells) and *STIM1*<sup>-/-</sup> (42 cells) HEK293-ACE2 cells after passive depletion of intracellular Ca<sup>2+</sup> stores with thapsigargin (TG – 1  $\mu$ M) in Ca<sup>2+</sup>-free external solution. SOCE was measured after replacing external solution with that containing 2 mM CaCl<sub>2</sub>. Bar graph on the right shows averaged baseline subtracted ER Ca<sup>2+</sup> stores (TG) and SOCE ( $\pm$  s.e.m.) from four independent experiments.

(D) Bar graph shows baseline Ca<sup>2+</sup> levels (as depicted by Fura-2 ratio)  $\pm$  s.e.m. in indicated cell types upon perfusion with extracellular solution containing either 2 mM or 20 mM CaCl<sub>2</sub>. Each dot represents data obtained from an independent experiment.

\*\*\**P*<0.0005 (two-tailed *t* test).

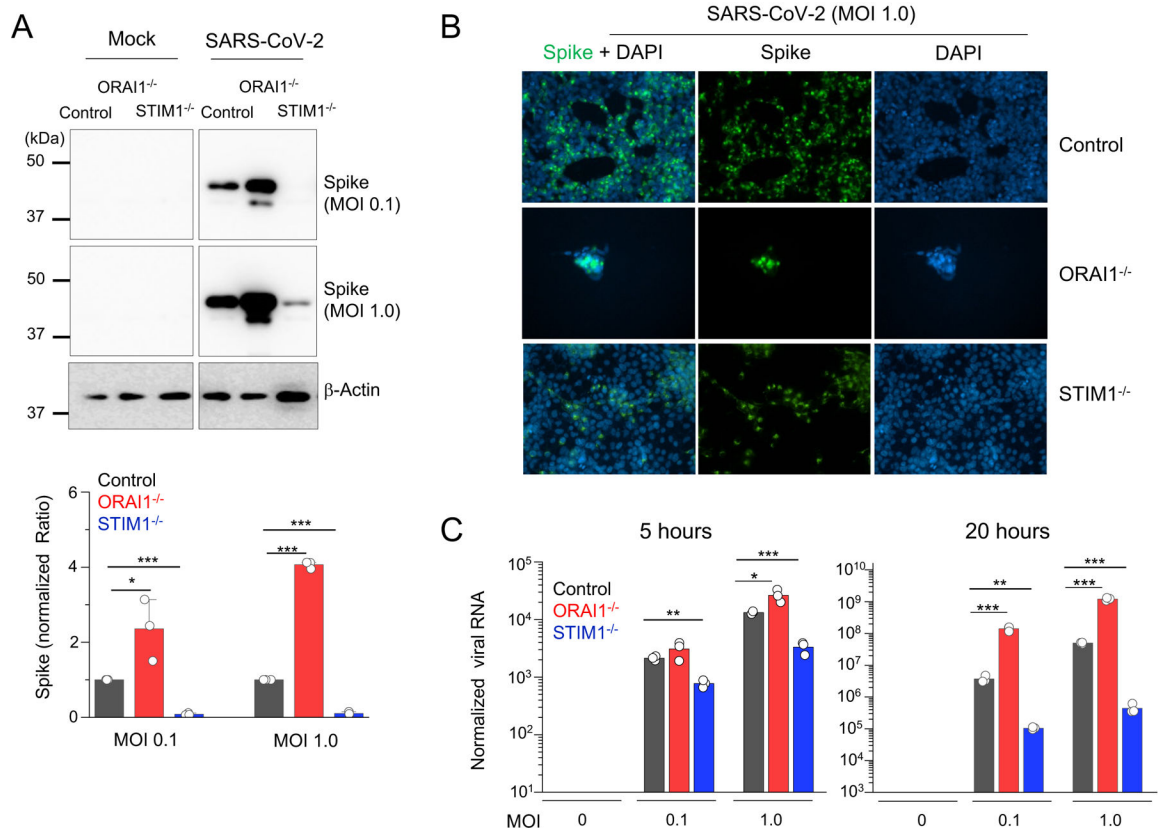


**Figure 2. Loss of ORAI1 or STIM1 affects cellular susceptibility to SARS-CoV-2 infection**

(A) Representative immunoblot showing expression of SARS-CoV-2 proteins in indicated HEK293-ACE2 cells under mock conditions or after infection with SARS-CoV-2 at indicated multiplicity of infection (MOIs). β-actin – loading control. Bar graph below shows densitometry analysis of normalized ratio of SARS-N-CoV-2 Spike protein to β-actin (± s.e.m.) from three independent experiments.

(B) Representative epifluorescence images (from two independent experiments) showing expression of spike protein (green) in control, *ORAI1*<sup>-/-</sup>, or *STIM1*<sup>-/-</sup> HEK293-ACE2 cells after infection with SARS-CoV-2 at MOI 1.0. Cells were co-stained with DAPI for detection of nuclei. *ORAI1*<sup>-/-</sup> HEK293-ACE2 cells were all detached due to high virus load.

(C) Quantitative RT-PCR analysis of viral genome from indicated cell types under mock conditions or after infection with SARS-CoV-2 at indicated MOI for 5 (left graph) or 20 (right graph) hours. Shown is one representative triplicate from two independent experiments.

\*  $P < 0.05$ , \*\*  $P < 0.005$ , \*\*\*  $P < 0.0005$  (two-tailed  $t$  test).

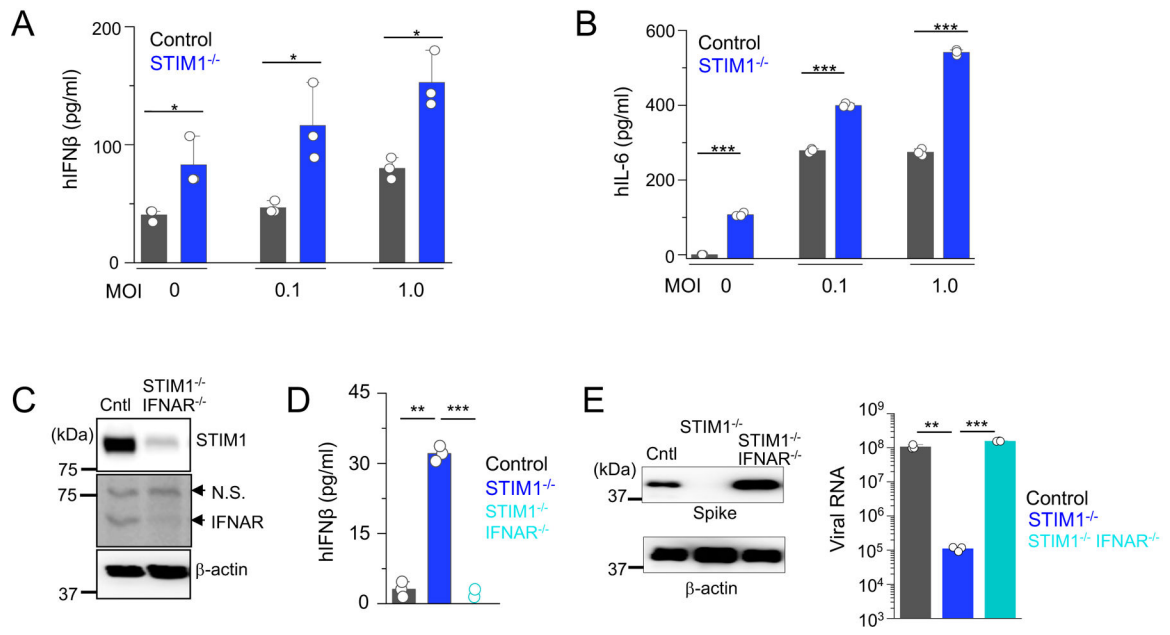


**Figure 3. Loss of STIM1 imparts resistance to SARS-CoV-2 infection by enhancing interferon  $\beta$  signaling pathway.**

(A) Levels of IFN- $\beta$  in culture supernatants from control or *STIM1*<sup>-/-</sup> HEK293-ACE2 cells under mock conditions or 20 hours after infection with SARS-CoV-2 at indicated MOIs.

(B) Levels of IL-6 in culture supernatants from control or *STIM1*<sup>-/-</sup> HEK293-ACE2 cells.

(C) Representative immunoblot showing expression of STIM1 and IFNAR1 in control HEK293-ACE2 cells or those deleted for both STIM1 and IFNAR1 using CRISPR/Cas9-mediated recombination.  $\beta$ -actin – loading control. Data are representative of two independent experiments. N.S., non-specific band.

(D) Levels of IFN- $\beta$  in culture supernatants from control, *STIM1*<sup>-/-</sup>, or *STIM1*<sup>-/-</sup> *IFNAR*<sup>-/-</sup> HEK293-ACE2 cells under resting conditions.

(E) Representative immunoblot showing expression of SARS-CoV-2 proteins in indicated HEK293-ACE2 cells under mock conditions or after infection with SARS-CoV-2 at MOI 0.1.  $\beta$ -actin – loading control. Data are representative of two independent infection experiments. Right - Quantitative RT-PCR analysis of viral genome from indicated cell types under mock conditions or after infection with SARS-CoV-2 at MOI 0.1 for 20 hours.

In bar graphs in panels (A), (B), (D), and (E) representative triplicates from two independent experiments are shown. \*  $P < 0.05$ , \*\*  $P < 0.005$ , \*\*\*  $P < 0.0005$  (two-tailed  $t$  test).

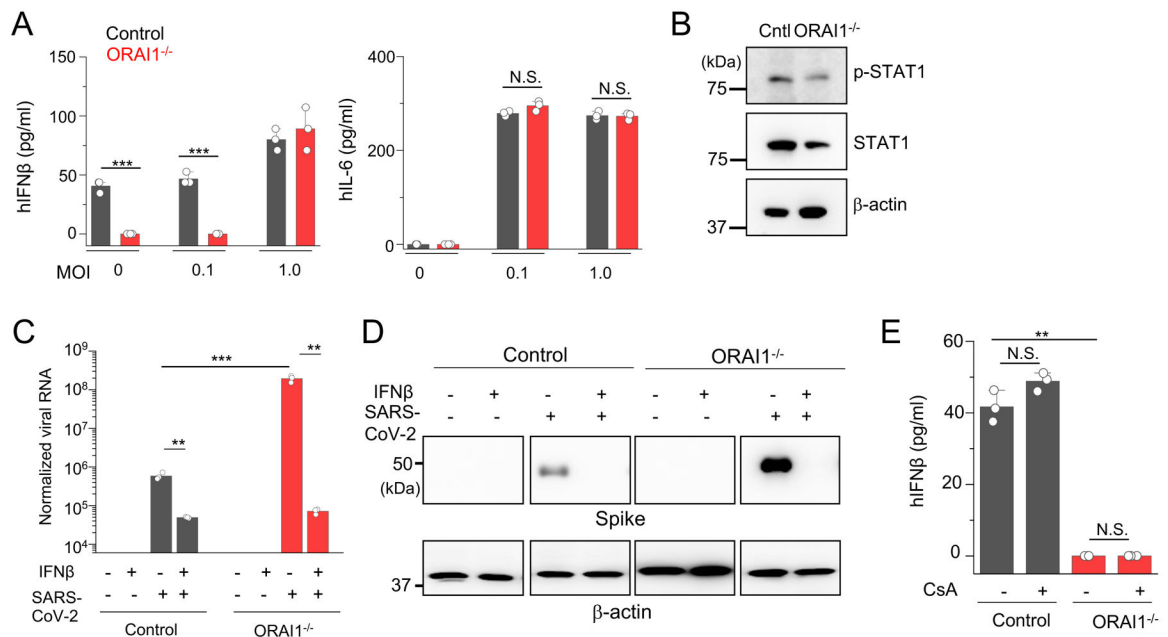


**Figure 4. Loss of ORAI1 imparts susceptibility to SARS-CoV-2 infection by abrogating baseline interferon  $\beta$  levels.**

(A) Levels of IFN $\beta$  and IL-6 in culture supernatants from control or *ORAI1*<sup>-/-</sup> HEK293-ACE2 cells under mock conditions or 20 hours after infection with SARS-CoV-2 at indicated MOIs.

(B) Representative immunoblot showing expression of phosphorylated STAT1 (p-STAT1) or total STAT1 in lysates from control or *ORAI1*<sup>-/-</sup> HEK293-ACE2 cells.  $\beta$ -actin – loading control. Data are representative of three independent experiments.

(C) Quantitative RT-PCR analysis of viral genome from indicated cell types with or without pre-treatment with 100 U/ml of IFN- $\beta$  (for 20 hours) under mock conditions or after infection with SARS-CoV-2 at MOI 0.1 for 20 hours. Data are representative of two independent infection experiments.

(D) Representative immunoblot showing expression of SARS-CoV-2 proteins in indicated HEK293-ACE2 cells with or without pre-treatment with 100 U/ml of IFN- $\beta$  (for 20 hours) under mock conditions or after infection with SARS-CoV-2 at MOI 0.1.  $\beta$ -actin – loading control. Data are representative of two independent infection experiments.

(E) Levels of IFN- $\beta$  in culture supernatants from control or *ORAI1*<sup>-/-</sup> HEK293-ACE2 cells with or without pre-treatment with 1 $\mu$ M cyclosporine A (CsA, 20 hours).

In bar graphs in panels (A), and (E) representative triplicates from two independent experiments are shown. \*  $P < 0.05$ , \*\*  $P < 0.005$ , \*\*\*  $P < 0.0005$  (two-tailed  $t$  test).

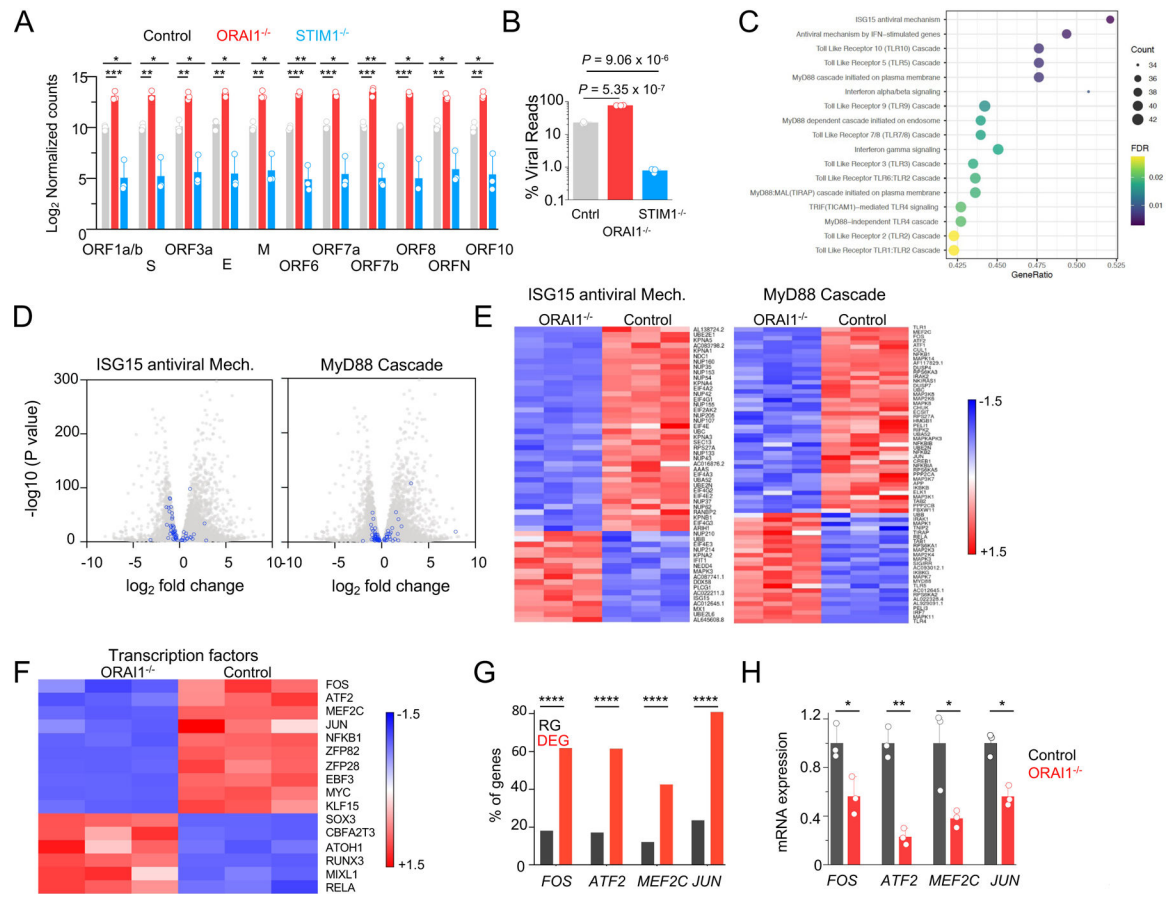


**Figure 5. Transcriptome analysis of control and *ORAI1*<sup>-/-</sup> HEK293-ACE2 cells.**

(A) Normalized read counts (log<sub>2</sub>) of SARS-CoV-2 RNA products, showing transcriptional enrichment of viral genes in SARS-CoV-2-infected cells when compared to uninfected cells.

(B) Bar graph shows proportion of total reads comprising SARS-CoV-2 transcripts in indicated cell types. The proportion of virus-aligned reads over total reads is shown for each sample. Error bars represent average ( $\pm$  s.d.m.) from three biological replicates.

(C) Dot plot visualization of enriched pathways in *ORAI1*<sup>-/-</sup> HEK293-ACE2 cells. Reactome pathway enrichment analysis was performed in PANTHER. The size of the dots represents the percentage of genes enriched in the total gene set, while its color represents the false discovery rate (FDR, p-adjusted) value for each enriched pathway.

(D) Volcano plots with all DEGs from *ORAI1*<sup>-/-</sup> and control mock (uninfected) samples in gray and the indicated gene sets of anti-viral ISG15 signaling (left) and MyD88 signaling (right) highlighted in blue (FDR < 0.01).

(E) Heat map illustrating z-scores as expression levels of the differentially expressed genes involved in antiviral signaling and MyD88 signaling pathways as show in panel D. Blue and red colors represent down- and up-regulated genes, respectively.

(F) Heat map depicting z-scores as expression levels of selected transcription factors differentially expressed between control and *ORAI1*<sup>-/-</sup> HEK293-ACE2 cells.

(G) Transcription factor binding sites at the promoters of genes (TSS  $\pm$  1.0 Kb) of the entire genome (from ChIP Atlas, RG) or among differentially expressed genes (DEG) in *ORAI1*<sup>-/-</sup>



HEK293-ACE2 cells. The hypergeometric  $P$  values (\*\*\*\*  $P < 0.0001$ ) were calculated by comparing background (complete gene sets of the reference host) to genes from DEGs to see enrichment of binding sites of indicated transcription factors.

**(H)** Quantitative RT-PCR analysis of the indicated genes from control and *ORAI1*<sup>-/-</sup> HEK293-ACE2 cells under resting conditions.

$P < 0.05$ , \*\*  $P < 0.005$ , \*\*\*  $P < 0.0005$  (two-tailed  $t$  test).

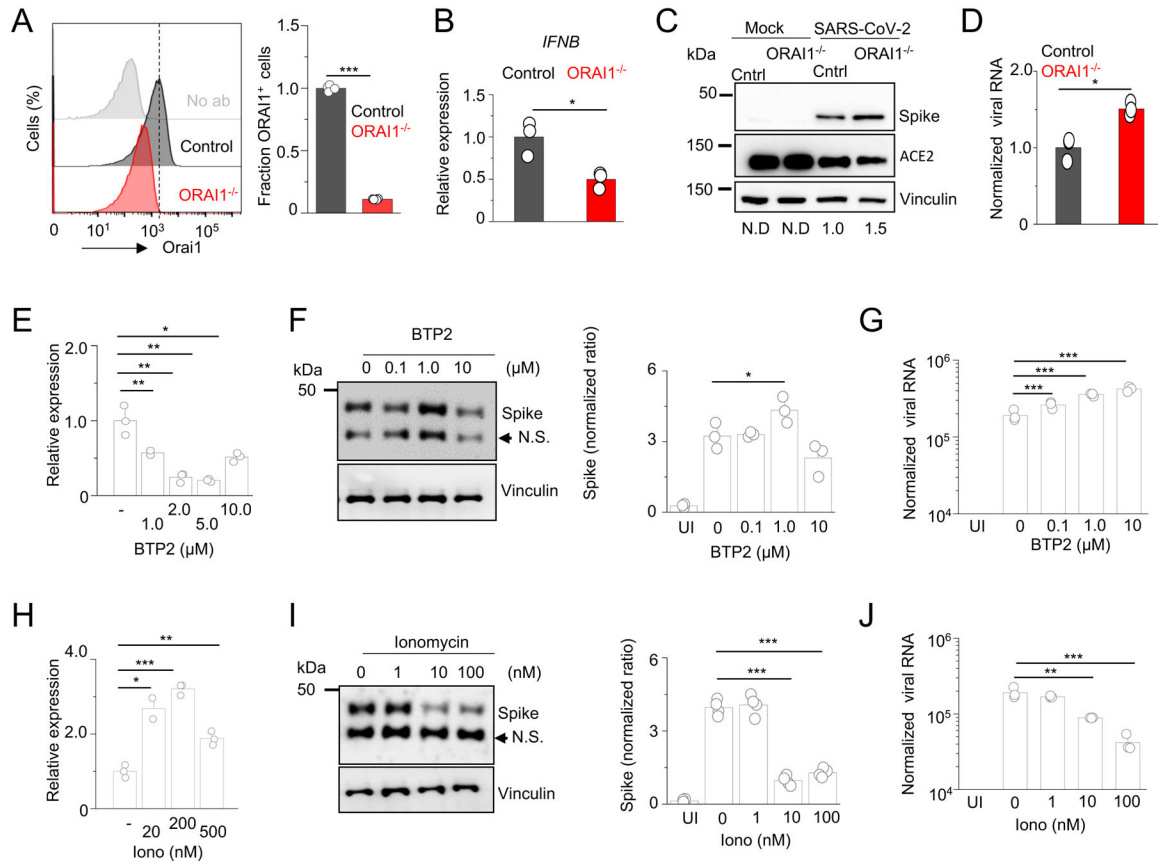


**Figure 6. Pharmacological alteration of homeostatic  $[Ca^{2+}]_i$  modulates host susceptibility to SARS-CoV-2**

(A) Representative histograms showing levels of total ORAI1 protein in control and *ORAI1*<sup>-/-</sup> A549-ACE2 cells after permeabilization and intracellular staining with anti-ORAI1 antibody. The bar graph shows average ( $\pm$  s.e.m.) from three independent experiments.

(B) Quantitative RT-PCR analysis for expression of *IFNB* transcripts in control or *ORAI1*<sup>-/-</sup> A549-ACE2 cells cultured in the presence of medium containing 10 mM  $CaCl_2$ . Data are representative of two independent experiments.

(C) Representative immunoblot showing expression of SARS-CoV-2 and ACE2 proteins in indicated A549-ACE2 cells under mock conditions or after infection with SARS-CoV-2 at indicated MOI 0.1. Vinculin – loading control. Numbers below indicate normalized fold change in ratio of Spike to vinculin. N.D – Not determined. Data is representative of two experiments.

(D) Quantitative RT-PCR analysis of viral genome from indicated A549-ACE2 cells after infection with SARS-CoV-2 at MOI of 0.1 for 20 h. Data is representative of two experiments.

(E) Quantitative RT-PCR analysis for expression of *IFNB* transcripts from A549-ACE2 cells pre-treated with vehicle or indicated concentrations of BTP2 for 24 h. Shown is one representative triplicate from two independent experiments.

**(F)** Representative immunoblot showing expression of SARS-CoV-2 proteins in A549-ACE2 cells pre-treated with vehicle or indicated concentrations of ORAI1 blocker BTP2 for ~24 h and infected with SARS-CoV-2 at MOI 0.1. Vinculin – loading control. UI – uninfected cells, N.S., non-specific band. Bar graph (right) shows densitometry analysis of normalized ratio of SARS-N-CoV-2 to vinculin ( $\pm$  s.e.m.) from technical replicates of two independent experiments.

**(G)** Quantitative RT-PCR analysis of viral genome from A549-ACE2 cells pre-treated with vehicle or indicated concentrations of ORAI1 blocker BTP2 for 24 h and infected with SARS-CoV-2 at MOI 0.1. Shown is one representative triplicate from two independent experiments.

**(H)** Quantitative RT-PCR analysis for expression of *IFNB* transcripts from A549-ACE2 cells pre-treated with vehicle or indicated concentrations of ionomycin (iono) for 24 h. Shown is one representative triplicate from two independent experiments.

**(I)** Representative immunoblot showing expression of SARS-CoV-2 proteins in A549-ACE2 cells pre-treated with vehicle or indicated concentrations of ionomycin for 24 h and infected with SARS-CoV-2 at MOI 0.1. Vinculin – loading control. UI – uninfected cells, N.S., non-specific band. Bar graph (right) shows densitometry analysis of normalized ratio of SARS-N-CoV-2 to vinculin ( $\pm$  s.e.m.) from technical replicates of two independent experiments.

**(J)** Quantitative RT-PCR analysis of viral genome from A549-ACE2 cells pre-treated with vehicle or indicated concentrations of ionomycin for 24 h and infected with SARS-CoV-2 at MOI 0.1. Shown is one representative triplicate from two independent experiments.

\*  $P < 0.05$ , \*\*  $P < 0.005$ , \*\*\*  $P < 0.0005$  (two-tailed *t* test).